BIOCHEMISTRY
including biophysical chemistry & molecular biology

Article

pubs.acs.org/biochemistry

Amyloid-Forming Proteins Alter the Local Mechanical Properties of Lipid Membranes

Kathleen A. Burke,[†] Elizabeth A. Yates,[†] and Justin Legleiter*[,†,‡,§]

[†]C. Eugene Bennett Department of Chemistry, [‡]WVnano Initiative, and [§]Center for Neurosciences, West Virginia University, Morgantown, West Virginia 26505, United States

Supporting Information

ABSTRACT: A diverse number of diseases, including Alzheimer's disease, Huntington's disease, and type 2 diabetes, are characterized by the formation of fibrillar protein aggregates termed amyloids. The precise mechanism by which aggregates are toxic remains unclear; however, these proteins have been shown to interact strongly with lipid membranes. We investigated morphological and mechanical changes in model lipid bilayers exposed to amyloid-forming proteins by reconstructing the tapping forces associated with atomic force microscopy (AFM) imaging in solution. Tip/sample tapping forces contain information regarding mechanical properties of surfaces. Interpretation of the mechanical changes in the bilayers was aided by numerical simulations of the entire AFM experiment. Amyloid-forming proteins disrupted distinct regions of the bilayer morphology, and these regions were associated with decreased Young's modulus and adhesive properties. These changes in bilayer mechanical properties upon exposure to amyloid-forming proteins may represent a common mechanism leading to membrane dysfunction in amyloid diseases.

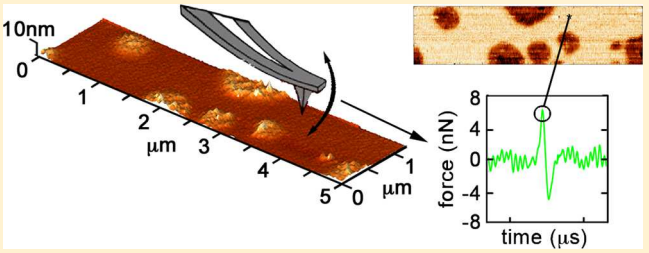

A vast number of diseases are characterized by the misfolding of specific proteins, causing these proteins to assemble into a wide array of extracellular and/or intracellular aggregates. Disease-associated protein aggregation often results in extended, β-sheet-rich, proteinaceous fibrillar structures, termed amyloids. These fibrils often have globular, soluble protein aggregate precursors, termed oligomers. These diseases include Alzheimer's disease (AD), Huntington's disease (HD), type 2 diabetes, and many others.[1] For example, one of the hallmarks of AD is the aggregation of the β-amyloid peptide (Aβ) into extracellular neuritic plaques,[2] and HD is caused by an expanded polyglutamine tract in the huntingtin (htt) protein that leads directly to its aggregation into inclusion bodies in affected neurons.[3] Amyloid deposits of amylin are a pathological characteristic of the pancreas in type 2 diabetes.[4]

The two-dimensional liquid environment of lipid bilayers can profoundly influence protein structure and dynamic properties, thereby influencing the aggregation state of amyloid-forming proteins.[5] A common factor modulating amyloid formation appears to be the presence of lipid membranes, as fibril formation has been shown to be accelerated in a membrane environment for several amyloid-forming proteins, including amylin[6] and Aβ.[7−11] While lipid membranes may play a role in facilitating aggregation,[12,13] such membranes may be direct targets of toxic mechanisms associated with amyloid formation, such as membrane permeabilization associated with altered bilayer structure due to sequestration of membrane components into aggregates[12,14−21] or the formation of unregulated pores.[22,23] Aβ is a cleavage product of the amyloid precursor protein (APP) and, as such, contains a portion of the APP transmembrane domain, which can facilitate Aβ's interaction with lipid membranes. The subcellular localization and interaction of htt-containing expanded polyQ domains with membranous surfaces have been well documented and suggest that these interactions play a role in HD pathogenesis.[24−28] Amylin has been shown to disrupt lipid bilayers by forming either defects[19] or pores.[29,30] The association of amyloid-forming proteins with cellular membranes may represent a common step associated with a variety of mechanisms of toxicity. The exact chemical composition and lipid constituents contained within a lipid membrane can heavily influence the aggregation process.[31] For example, cholesterol[11,20,32,33] and oxysterols[34] have been shown to modulate the interaction of Aβ with lipid membranes. The interaction of amyloid-forming proteins with lipid membranes may also play an important role in modulating the effectiveness of small molecules designed to inhibit aggregation, as was demonstrated with (−)-epigallocatechin gallate (EGCG), which inhibits amyloid formation in the absence of lipid membranes[35,36] but is less effective at a phospholipid interface.[37]

Here, we investigate the interaction of four amyloid-forming proteins, Aβ, htt, a synthetic polyQ peptide, and amylin (Figure S1 of the Supporting Information), with total brain lipid extract (TBLE) bilayers. These peptides represent two potentially different mechanisms of interaction with lipid membranes. The

Received: August 8, 2012
Revised: January 17, 2013
Published: January 18, 2013

ACS Publications © 2013 American Chemical Society

interaction of Aβ with lipid bilayers is driven by an amphipathic character associated with being a fragment of a transmembrane protein.[38] htt, synthetic polyQ peptide, and amylin all contain α-helical lipid binding domains.[39,40] In particular, we used a variation of in situ tapping mode atomic force microscopy (AFM), and scanning probe acceleration microscopy (SPAM), which allowed us to simultaneously determine the morphological and mechanical impact of exposure to amyloid-forming proteins on the bilayers. Tapping mode AFM is a well-established imaging technique capable of nanoscale resolution; however, the time-resolved tip/sample forces associated with tapping mode AFM contain information concerning mechanical surface properties, i.e., adhesion, rigidity, energy dissipation, and compressibility. The SPAM technique is able to reconstruct the tapping force for every cantilever oscillation cycle during imaging by taking the second derivative (or acceleration) of the cantilever deflection signal after Fourier transform-based filtering.[41] Furthermore, SPAM can operate in aqueous solution, making it highly applicable to biologically relevant samples. Numerical simulations of the entire tapping mode AFM scanning process are also provided to assist in the interpretation of the acquired tip/sample tapping forces.

MATERIALS AND METHODS

Preparation of Defect-Free Bilayer Patches. Lyophilized total brain lipid extract (porcine) was purchased from Avanti Polar Lipids (Alabaster, AL) and resuspended in phosphate-buffered saline (PBS) (pH 7.3) at a concentration of 1 mg/mL. By using an acetone/dry ice bath, bilayers and multilayer lipid sheets were formed by five cycles of a freeze−thaw treatment.[8] Vesicle formation within the lipid suspensions was promoted by bath sonication for 30 min. All experiments were performed with the same lot of lipids. Twenty-five microliters of the suspended vesicle solution, diluted with 25 μL of PBS (pH 7.3), was added directly to the AFM fluid cell and the cell placed onto freshly cleaved mica. Vesicles were allowed to absorb to the mica and fuse together to form a supported bilayer (40 μm × 40 μm) that was relatively defect-free as assessed by an AFM image (Figure S2 of the Supporting Information). Once the bilayer formed, two or three washes with PBS were performed to remove excess lipid vesicles. For these experiments, the lipid:peptide ratio was approximately between 5 and 15. The uncertainty is due to several factors. First, TBLE is a complex mixture of lipids, so there is not a straightforward way to calculate the moles of lipid components. Second, despite efforts to be as consistent as possible, the efficiency of the washing step after formation of the bilayer may vary, resulting in slightly different amounts of total lipid in the fluid cell.

Preparation of Protein Samples. Wild-type Aβ_{1-40} (AnaSpec, San Jose, CA) and human amylin(1−37) (AnaSpec) were prepared using published protocols that result in monomeric solutions.[19,42−44] Aβ_{1-40} and amylin were treated separately with hexafluoro-2-propanol (HFIP) to dissolve preexisting aggregates and seeds. The resulting solutions of Aβ_{1-40} or amylin were placed under vacuum to remove the HFIP, resulting in peptide films. Aβ_{1-40} films were resuspended in 10 μL of dimethyl sulfoxide (DMSO) and vortexed to make 2000 μM stock solutions, which were dissolved directly into PBS buffer (pH 7.3) to a final concentration of 20 μM. The amylin films were resuspended in PBS and vortexed, resulting in a final concentration of 50 μM. htt exon1−51Q was purified from *Escherichia coli* as a glutathione *S*-transferase (GST)−htt fusion protein by protocols that result predominately in monomeric protein.[45,46] The fusion proteins were purified from lysates using a BioLogic LP system (Bio-Rad) equipped with a GST affinity column. Gel electrophoresis was used to determine purity and to verify the relevant fractions. The GST moiety was cleaved with Factor Xa (Promega, Madison, WI), which initiates aggregation. Prior to the addition of the cleaving agent, solutions of GST−htt fusion proteins were centrifuged at 20000*g* for 30 min at 4 °C to remove any preexisting aggregates. The concentration of htt exon1−51Q was determined using a Bradford assay, and solutions of htt exon1−51Q were prepared, with a final concentration of 20 μM. Synthetic polyQ peptides (Keck Biotechnology Resource Laboratory, New Haven, CT) were dissolved for 3 h in a 1:1 mixture of trifluoroacetic acid (TFA) and HFIP to a concentration of 0.5 mg/mL, which results in a monomeric stock based on published protocols.[47] After the mixture had been vortexed, the solvent was evaporated off, producing a thin peptide film. The polyQ peptide film was resuspended in ultrapure water adjusted to pH 3 with TFA to a concentration of 2.0 mg/mL. This stock solution was diluted in PBS to a final concentration of 20 μM and a pH of 7.3. For Aβ, amylin, and polyQ peptide preparations, aliquots of each solution were spotted on mica as soon as they were prepared to verify the absence of aggregates via AFM imaging in air. Bovine serum albumen (BSA) (Thermo Scientific) was diluted in PBS to a final concentration of 20 μM and used directly.

AFM and SPAM Imaging Conditions. In situ AFM experiments were performed with a Nanoscope V MultiMode scanning probe microscope (Veeco, Santa Barbara, CA) equipped with a closed-loop "vertical engage" J-scanner and a sealable tapping fluid cell. Images were acquired with V-shaped oxide-sharpened silicon nitride cantilevers (Veeco) with nominal spring constants of ∼0.5 N/m and a nominal tip radius of <10 nm. Scan rates were set at 1−2 Hz with cantilever drive frequencies ranging from ∼8 to 10 kHz. The free amplitude of the cantilever was ∼25 nm, and the tapping amplitude was set at 70% of this free amplitude. For SPAM experiments, 5 μm × 1.25 μm images were captured with 256 × 64 pixel resolution. Using a signal access module (Veeco) and CompuScope 14100 data acquisition card (Gage, Lachine, QC), cantilever deflection trajectories were captured at 2.5 MS/s and 14 bit resolution with a range of 2 V. The captured cantilever trajectory was filtered using a Fourier transform-based harmonic comb filter.[41] The second derivative of the resulting filtered cantilever deflection trajectory was taken and multiplied by the effective mass, m_{eff}, of the cantilever to obtain the time-resolved-based tapping force between the tip and sample. m_{eff} was determined using a thermal tuning method,[48] performed in solution, yielding the spring constant and resonance frequency of the cantilever, which can be used to determine m_{eff} based on the following equation:

$$m_{eff} = \frac{k}{\omega^2} \tag{1}$$

Numerical Simulations of the Complete AFM Experiment. The cantilever motion was described as a single degree of freedom damped driven harmonic oscillator.[49,50]

$$m_{eff}\ddot{z} + b\dot{z} + k[z - D_0 + a_0 \sin(\omega t)] = F_{ext} \tag{2}$$

where m_{eff} is the effective mass of a cantilever, b is the damping coefficient, k is the cantilever spring constant, a_0 is the drive amplitude, ω is the drive frequency, D_0 is the resting position of

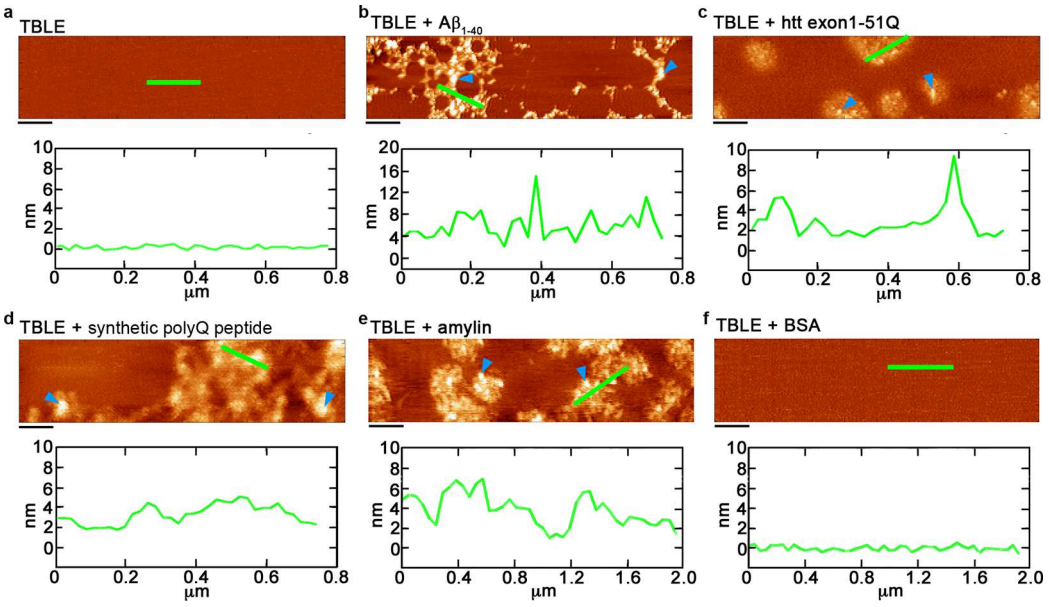

Figure 1. Amyloid-forming proteins disrupt TBLE bilayers. Representative two- and three-dimensional in situ AFM images of TBLE bilayers that were exposed to (a) control buffer, (b) 20 μM wild-type Aβ_{1-40}, (c) 20 μM htt exon1−51Q, (d) 20 μM synthetic polyQ peptide, (e) 50 μM amylin, and (f) 20 μM bovine serum albumin (as a control). The green lines in the two-dimensional images correspond to the height profiles below the AFM images. Arrows indicate discrete aggregate complexes that may represent oligomeric species. The scale bar in panels a−d represents 500 nm, and the scale bar in panels e and f represents 1000 nm.

the cantilever base, F_{ext} is the tip/sample force, and z is the position of the cantilever with respect to the surface. In tapping mode, the tip/surface separation distance changes as the cantilever oscillates. While the tip and surface are not in contact for the majority of the oscillation cycle (noncontact regime), the tip intermittently contacts (or taps) the surface during each cycle. In solution, the AFM tip in the proximity of a surface would experience van der Waals forces and electric double-layer forces, which can be described by the Derjaguin−Landau−Verway−Overbeek (DLVO) theory.[51] Our experimental system, however, has a high salt concentration in the buffer, resulting in a short Debye length and negligible forces arising from the electric double layer.[52] As a result, the external force associated with the noncontact regime was approximated using the van der Waals interaction between a sphere and flat surface:[53]

$$F_{ext} = -\frac{AR_{tip}}{6z^2} \quad \text{for} \quad z > a_{DMT} \tag{3}$$

where A is the Hamaker constant, R_{tip} is the tip radius, and a_{DMT} is the interatomic distance parameter of a Derjaguin−Muller−Toporov (DMT) potential.[54] When the separation distance between the tip and surface is less than or equal to a_{DMT}, the tip is in contact with the surface, and the external force was modeled with a DMT potential

$$F_{ext} = \frac{4}{3\pi\kappa_{eff}}\sqrt{R}(a_{DMT} - z)^{3/2} - \frac{AR_{tip}}{6a_{DMT}^2} \quad \text{for} \quad z \le a_{DMT} \tag{4}$$

with

$$\kappa_{eff} = \frac{1 - \nu_{tip}^2}{\pi E_{tip}} + \frac{1 - \nu_{sample}^2}{\pi E_{sample}} \tag{5}$$

where E_{tip}, E_{sample}, ν_{tip}, and ν_{sample} are the Young's moduli and Poisson coefficients of the tip and sample, respectively.

To simulate the entire scanning process, we implemented a feedback loop containing an integral gain in the model. In practice, the cantilever deflection, rather than the position with respect to the surface, is monitored experimentally. As a result, the feedback loop in the model monitored the oscillation amplitude of the deflection (y) of the cantilever, which is related to the position by

$$y = z - D_0 + a_0 \quad \sin(\omega t) \tag{6}$$

The measured amplitude of the deflection signal was compared to a specified set point amplitude, and the cantilever position relative to the surface was adjusted to maintain the set point. The feedback loop feature can be used to simulate the process of acquiring an AFM scan line in which the surface topography is variable. The resulting model is capable of capturing several features of the cantilever deflection signal and tip/sample force (Figure S3 of the Supporting Information).[55,56]

RESULTS AND DISCUSSION

Amyloidogenic Proteins Alter Membrane Morphology. To determine the impact of exposing lipid membranes to amyloid-forming proteins, supported TBLE bilayers were used as a model surface. TBLE is comprised of a physiologically relevant ratio of membrane components (cholesterol, gangliosides, sphingolipids, isoprenoids, and both acidic and neutral phospholipids), providing a relevant model surface. The supported bilayers were formed by vesicle fusion on freshly cleaved mica[57] and systematically exposed to a variety of amyloid-forming proteins (Aβ_{1-40}, htt exon1−51Q, synthetic polyQ peptide, or amylin). Observations were limited to 40 μm × 40 μm patches of bilayer that were defect-free, at a scale determined by AFM analysis, prior to exposure to amyloid-forming proteins. A freshly prepared bilayer was used in each experiment, and the addition of protein indicated our zero time

dx.doi.org/10.1021/bi301070v | Biochemistry 2013, 52, 808−817

point for exposure. No additional protein was added after the initial injection. Each protein was freshly prepared and was in a predominately monomeric state upon initial injection, although some small aggregates may have been present. Control experiments were performed by exposing TBLE bilayers to protein-free solutions that were identical to vehicle solvents used for each protein. None of these vehicle solutions altered the morphology or mechanics of the TBLE bilayer as assessed by AFM.

A freshly formed bilayer had a smooth appearance with a root-mean-square (rms) roughness of 0.06 ± 0.03 nm. Initially, when the lipid bilayer was exposed to freshly prepared solutions of Aβ_{1-40} (20 μM), htt exon1−51Q (20 μM), synthetic polyQ peptide (20 μM), or amylin (50 μM), patches of increased surface roughness developed, indicating disruption of the bilayer structure (Figures 1 and 2). When the rms roughness of

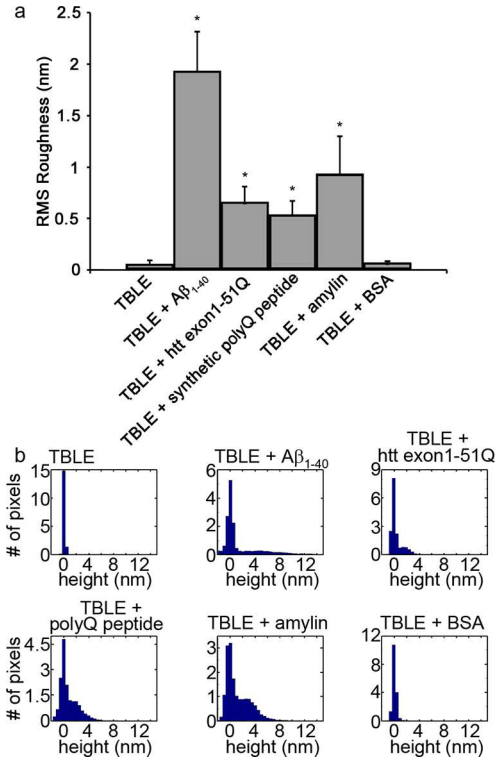

Figure 2. Exposure to amyloid-forming proteins causes increased surface roughness in TBLE bilayers. (a) Root-mean-square (rms) surface roughness analysis of TBLE bilayers before (TBLE) and after exposure to Aβ_{1-40}, htt exon1−51Q, synthetic polyQ peptide, and amylin induced significant (*p < 0.01) roughening of the TBLE bilayer, as assessed by a t test with n = 5. The rms roughness measurements were restricted to disrupted regions of the surface. (b) Height histograms of every pixel contained in the AFM images presented in Figure 1. Exposure to BSA served as a control.

these regions was measured (excluding the unperturbed regions of the image to normalize for the surface area actually occupied by roughened morphology), the increased roughness induced in the bilayer by all four amyloid-forming proteins was statistically significant (p < 0.05) (Figure 2a). Histograms of the height values associated with every pixel within the region also demonstrate that the bilayer morphology was significantly altered upon exposure to the amyloid-forming proteins (Figure 2b). TBLE not exposed to any protein or TBLE exposed to BSA had tight distributions of height values centered around 0 nm, as zero height corresponds to the top of the unperturbed bilayer. With exposure to amyloid-forming proteins, the histogram deviates from zero to larger values of height, indicating the extent of the bilayer roughness. Small aggregate complexes were often observed within these roughened domains for each protein, but fibrils were not observed (Figure 1, blue arrows). These aggregate complexes were globular in morphology. While these complexes are most likely comprised of both peptide and lipid components, they may represent discrete oligomers. The concentrations used in this study are much higher than those typically observed in vivo for these proteins. This was done to allow for observations over an experimentally feasible length of time. As aggregation is highly dependent on concentration, this must be taken into consideration when interpreting these results.

The disrupted regions of bilayers exposed to Aβ_{1-40} took ∼12−18 h to develop and exhibited the largest surface roughness (rms = 1.95 ± 0.38 nm) (Figure 1b). Aβ_{1-40} formed aggregate complexes (4−16 nm in height) larger than those formed by the other amyloid-forming proteins in the presence of the bilayer. Other reported globular aggregates of Aβ tend to be smaller than the observed aggregate complexes. Amyloid-derived diffusible ligands (ADDLs) have been observed to be 3−5 nm in height,[58] which is on the small end of the range of aggregates observed in this study. Much smaller Aβ oligomers are commonly observed, such as Aβ*56, which has been reported to be ∼1 nm in height.[59] The larger size of the observed complexes may indicate that either lipid components indeed accumulate within the complex or the TBLE lipid environment is promoting the formation of a larger globular aggregate.

Bilayer disruption occurred within 10−25 min of exposure to htt exon1−51Q (Figure 1c). Despite the apparent more aggressive interaction of htt exon1−51Q with the bilayer, the associated rms roughness with disruption was smaller (0.66 ± 0.15 nm) and the size of observed aggregate complexes was typically smaller (2−10 nm in height) compared to those of Aβ_{1-40}. While these aggregate complexes associated with htt exon1−51Q may contain some lipid components, they were similar in size to oligomers observed for a htt exon1 construct with 53Q repeats[60] and to htt exon1 purified from transgenic mice.[61] While the rate of interaction with the bilayer appeared to be slower (1−3 h), the synthetic polyQ peptide interacted with the membrane in a fashion similar to that of htt exon1−51Q, with an rms roughness of 0.54 ± 0.13 nm and aggregate complex heights ranging between 2 and 5 nm (Figure 1d). The slower apparent rate of aggregation on the bilayer of the synthetic polyQ peptide compared to the htt exon1−51Q protein was potentially caused by the length of the polyQ domain, which has been shown to alter the rate of aggregation.[60]

As amylin interacted with the bilayer with the slowest apparent rate, the concentration was increased to 50 μM, which resulted in membrane disruption within 3 h (Figure 1e). The rms roughness of the amylin-induced disrupted bilayer regions was 0.94 ± 0.36 nm, and the observed aggregate complexes were ∼2−7 nm in height. Similarly sized oligomers of amylin (3.6 nm) were reported from aggregation studies performed in the presence of a DOPC/DPPC/Chol lipid bilayer system, but this was observed at a much lower concentration (1 μM) and after a longer incubation time (30 h).[62] These aggregate complexes that formed on the TBLE bilayer were also much larger than oligomers of amylin that are commonly observed

dx.doi.org/10.1021/bi301070v | Biochemistry 2013, 52, 808−817

during the lag phase of aggregation in the absence of a lipid membrane.[62,63]

Complicating the comparison of these observed aggregates with those reported in the literature is the fact that the heights of the aggregate complexes associated with each protein were measured with respect to the bilayer surface. As a result, the actual heights of the aggregate complexes associated with the exposure to all four peptides may be larger than measured here if the complex is fully or partially inserted into the bilayer. As a control, bilayers were exposed to 50 μM bovine serum albumin (BSA), and no bilayer disruption (rms roughness of 0.07 ± 0.01 nm) or protein aggregation was observed over 24 h (Figure 1f).

The differences in the magnitude of roughening caused by each protein may be attributable to the mechanism of lipid binding associated with each protein. The random coil in the transmembrane and extracellular domains of Aβ can result in deeper insertion into the bilayer, resulting in a larger roughness measurement. The amphiphilic α-helix in htt exon1−51Q, synthetic polyQ peptide, and amylin allow for lipid binding with less insertion into lipid membranes when compared to that with Aβ_{1-40}.[21] Partial insertion of amylin into lipid membranes, stabilizing its α-helical character, has been suggested by molecular dynamics simulations.[64] The lateral morphology of the disrupted regions of the bilayer associated with the different amyloid-forming proteins varied. The disrupted regions of the bilayer associated with Aβ_{1-40} were often interconnected by meandering, elongated regions. htt exon1−51Q and amylin were associated with round regions of increased surface roughness that were typically between 300 and 500 nm in diameter. The synthetic polyQ peptide also formed these round regions of disruption, but often these regions were as large as 1−2 μm in diameter and generally were fewer in number.

Collectively, these observations suggest that the disruption of membrane structure is a common feature of the interaction between amyloid-forming proteins and lipid bilayers. This disruption should alter the local mechanical properties of the bilayer, compromising its ability to function properly as a membrane. Mechanical properties of lipids have long been thought to correlate with dysfunction and disease[65−67] because it is hypothesized that elasticity and adhesion of membranes directly influence cell stability. Cell and/or lipid permeability correlating with dysfunction has previously been suggested with Aβ,[68,69] mutant htt,[28,70] and amylin.[71,72] As a result, analysis of the tip/sample tapping forces was conducted to determine the impact of these amyloid-forming proteins on the mechanical properties of the bilayer.

Features of the Time-Resolved Tip/Sample Tapping Forces Can Be Used To Measure Mechanical Properties. It has been established that features of the time-resolved tip/sample force associated with tapping mode AFM are dependent on the mechanical properties of the sample.[41,52,73−80] While AFM topography images of protein/lipid bilayer systems were being obtained, the cantilever deflection signal was captured and used to recover the time-resolved tip/sample tapping force. Features of the force associated with tapping events changed during the imaging processes, suggesting differences in mechanical properties along the surface. In particular, the maximal tapping force (F_{max}) and minimal tapping force (F_{min}) per oscillation cycle varied. F_{max} is defined as the peak or largest positive force experienced between the tip and surface during one tapping event, and F_{min} is defined as the largest negative force experienced between the tip and surface (Figure S3a of the Supporting Information). To demonstrate the impact of surface properties on the tip/sample force interaction associated with tapping mode AFM in fluids and to aid in the interpretation of these force interactions, numerical simulations of the entire imaging process were performed as described in Materials and Methods.[41,55,56]

For changes in the tip/sample force to be useful in determining the mechanical properties of lipid bilayers disturbed by amyloid-forming proteins, the tip/sample tapping force must be independent of the surface roughness. To determine the role of surface roughness on tip/sample tapping forces, simulations were performed using 500 nm long model surfaces that consisted of two regions of rms roughness of 0.1 nm (similar to the undisturbed bilayer) flanking a region in which the rms roughness was varied (0.5 to 2.0 nm) in successive simulations (Figure S4 of the Supporting Information). The range of rms roughness used in these simulations was comparable to that observed for bilayers disrupted by amyloid-forming proteins. As there is an inherent response time associated with the ability of the feedback loop to restore the tapping amplitude when the tip encounters an abrupt change in surface morphology, the tapping force trajectory appears choppier when the rms roughness increases. However, the average F_{max} and F_{min} do not change as a function of rms roughness (Figure 3a,b). This indicates that as long as the feedback loop is optimized, changes in tapping forces are not dependent on sample topography.

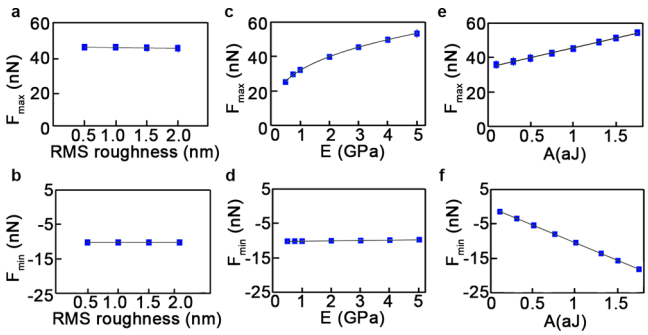

Figure 3. On the basis of numerical simulations, time-resolved tip/sample tapping forces can be used to measure local surface properties of surfaces, independent of morphology. (a) F_{max} and (b) F_{min} plotted as a function of rms roughness. (c) F_{max} and (d) F_{min} plotted as a function of Young's modulus. (e) F_{max} and (f) F_{min} plotted as a function of the Hamaker constant.

After establishing that changes in F_{max} and F_{min} are independent of surface topography, we performed simulations to determine how the relative rigidity of the surface and its adhesion to the AFM probe altered features of the tip/sample force interaction. Changes in the rigidity of a surface can be modeled by changing the Young's modulus of the sample (E_{sample} in eq 5). As the surface free energy (and adhesive force) between the tip and surface is related to the Hamaker constant by

$$\gamma = \frac{A}{24\pi a_{DMT}} \approx \frac{A}{2.1 \times 10^{-21}} \quad (7)$$

the adhesive interaction between the tip and surface can be modeled by changing the value of the Hamaker constant. For these simulations, 500 nm long model surfaces that contained a region in which the mechanical properties of the surface could be changed in successive simulations were used. This variable

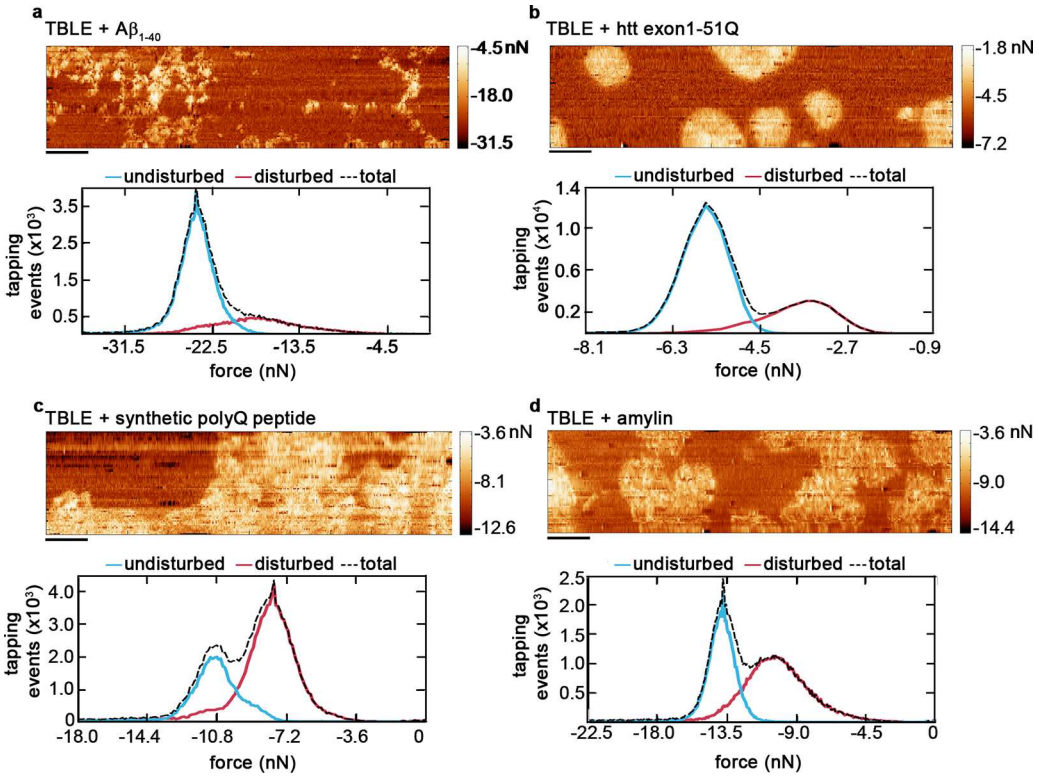

Figure 4. Lipid bilayers exposed to amyloid-forming proteins adhere less to the AFM probe, based on changes in the minimal tapping force. A series of F_{min} images and histograms of every tapping event associated with capturing AFM imaging of TBLE bilayers exposed to (a) Aβ_{1-40}, (b) htt exon1−51Q, (c) synthetic polyQ peptide, and (d) amylin are shown. These F_{min} images correspond to the topographical images presented in Figure 1. The scale bar in panels a−c represents 500 nm, and the scale bar in panel d represents 1000 nm.

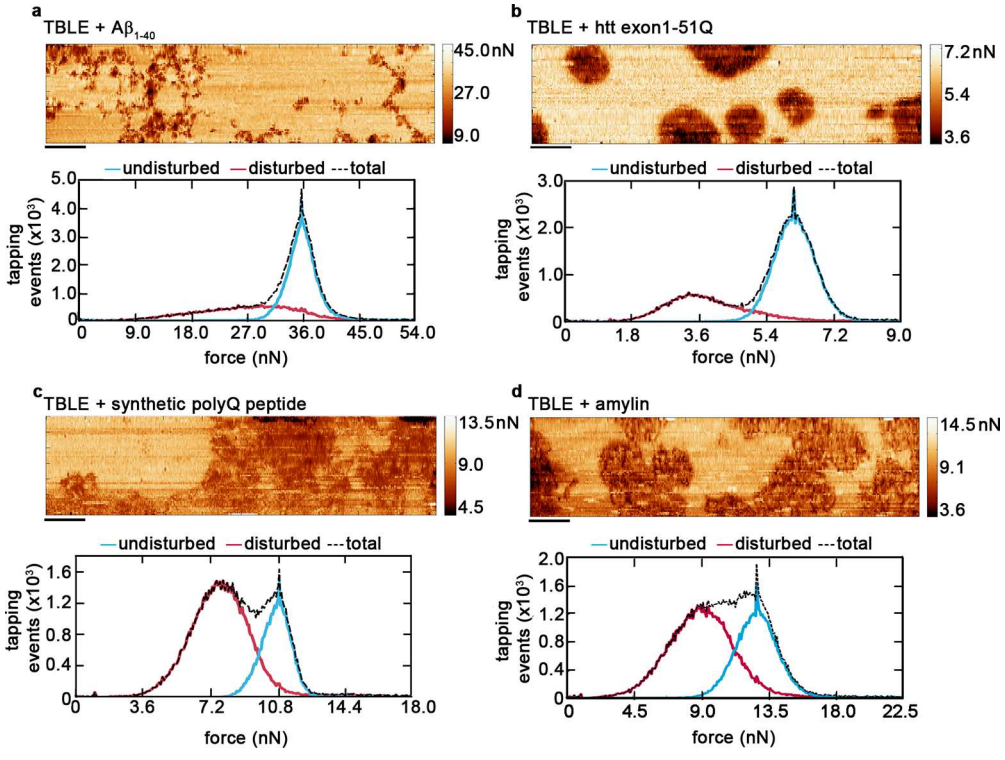

Figure 5. Exposure to amyloid-forming proteins softens lipid bilayers, based on changes in the maximal tapping force. A series of F_{max} images and histograms of every tapping event associated with capturing AFM imaging of TBLE bilayers exposed to (a) Aβ_{1-40}, (b) htt exon1−51Q, (c) synthetic polyQ peptide, and (d) amylin are shown. These F_{max} images correspond to the topographical images presented in Figure 1. The scale bar in panels a−c represents 500 nm, and the scale bar in panel d represents 1000 nm.

dx.doi.org/10.1021/bi301070v | *Biochemistry* 2013, 52, 808−817

region was flanked by regions that had a Young's modulus of 5.5 GPa and a Hamaker constant of 1.0 aJ. First, a series of simulations were run with the Young's modulus systematically increasing from 0.5 to 5 GPa in the variable region (the Hamaker constant was not changed) (Figure S5 of the Supporting Information). Increasing the Young's modulus results in a less compliant surface and a reduction in the constant, κ_{eff}, in eq 5. As a result, F_{max} increased in magnitude with larger values of the sample Young's modulus with a power law dependence (Figure 3c). F_{min} was independent of changes in the surface Young's modulus (Figure 3d). Next, a series of simulations were run with various values of the Hamaker constant (0.1−1.75 aJ) in the variable region of the model surface, and changes in F_{max} and F_{min} were observed (Figure S6 of the Supporting Information). As the Hamaker constant was increased, the attractive component of the tip/sample force became larger, and the magnitude of F_{min} increased (became more negative) in a linear fashion (Figure 3e). The larger attractive force also caused the tip to push deeper into the surface. As a result, the Hertzian portion of the tip/sample force during contact increased, causing F_{max} to increase in magnitude linearly with larger Hamaker constants (Figure 3f). Collectively, the simulations with varying values of the Hamaker constant or Young's modulus demonstrated that unique features of the tip/sample tapping force can be used to determine relative changes in the mechanical properties of the bilayer surface.

Amyloidogenic Proteins Alter the Mechanical Properties of Lipid Bilayers. To elucidate the impact of amyloid-forming proteins on lipid bilayers, we spatially analyzed the mechanical properties of the membranes on the basis of the time-resolved tip/sample imaging forces associated with tapping mode AFM. To accomplish this, we captured the entire tip deflection trajectory while obtaining an entire AFM image and converted the trajectory into the force interaction by SPAM. This allowed for specific tapping events to be correlated with morphological features of the surface. Spatially resolved maps of F_{min} (Figure 4) and F_{max} (Figure 5) that correspond to each topography image in Figure 1 of lipid bilayers exposed to amyloid-forming proteins were generated. The force images have distinct contrast between the undisturbed regions of the bilayer and the disrupted regions of the bilayer associated with all of the tested amyloid-forming proteins. Histograms of F_{min} and F_{max} for every tapping event can be sorted on the basis of topography images, so that every individual tapping event can be associated with specific regions in the surface. The domains in which proteins have associated with lipid, resulting in disruption, were associated with smaller magnitudes of both F_{min} and F_{max} compared to those of the undisturbed lipid domains. On the basis of simulations, there are several potential implications of these changes in the tip/sample force interaction associated with disrupted regions of the bilayer. The shifts in F_{min} and F_{max} were independent of the rougher morphology caused by the amyloid-forming proteins. As F_{min} was not altered by changes in the Young's modulus of the surface in the simulation, the observed shifts in F_{min} associated with exposure to amyloid-forming proteins were primarily due to a weakened adhesive interaction between the disrupted regions of the bilayer and the AFM tip. The shifts in F_{max} associated with disrupted regions of the bilayer are potentially related to changes in the bilayer's Young's modulus and/or the Hamaker constant associated with the interaction between the tip and surface. Simulations suggested that shifts in F_{max} due to changes in the surface free energy can be estimated from the observed change in F_{min}. Upon comparison of the results associated with F_{min} and F_{max}, the observed shift in F_{max} could not be completely accounted for by what would be expected on the basis of the observed shift in F_{min}. As a result, a portion of the observed decrease in F_{max} associated with disrupted regions of the bilayer can be associated with a decreased Young's modulus. Collectively, these results indicate that interaction between lipid bilayers and amyloid-forming proteins results in regions of altered membrane morphology (increased roughness) and mechanical properties (decreased Young's modulus of the bilayer and a weakened adhesive interaction between the tip and surface).

A potential explanation for these observed changes in bilayers exposed to amyloid-forming proteins is a decrease in the efficiency of the packing of the lipid components within the bilayer in response to protein insertion or binding and aggregation. This would lead to a rougher bilayer that is more easily compressed and a decrease in the number of potential hydrogen bonds formed between the tip and bilayer surface, leading to the weaker adhesive interaction. Previous studies highlight the effects lateral tension has on lipid structure and stability.[81,82] These studies suggest that because of the material properties of the lipid bilayer (thickness, intrinsic curvature, and Young's modulus) the membrane can serve as an allosteric regulator of membrane protein function. Furthermore, lipids naturally compress and/or stretch to minimize the interaction between hydrophobic domains of a transmembrane protein and the aqueous environment. Thus, once the amyloid-forming proteins associate with the bilayer, the bilayer may stretch itself to minimize the hydrophobic effect, allowing more space between the two tail ends of the lipid leaflets. A larger space between the two leaflets would be consistent with our results because this would result in greater compressibility. The primary limitation associated with the use of supported TBLE bilayers is the potential that interactions with the underlying mica substrate would influence the physical properties of the bilayer. While there is generally a thin water gap (~0.2−1 nm) between the substrate and the supported bilayer,[83−85] extensive hydrodynamic coupling between the bilayer and the substrate is still possible, reducing the diffusion coefficient of the supported bilayer.[86] As there is an apparent link between compressibility and lateral fluidity,[87] hydrodynamic coupling with mica may result in an altered compressibility of the bilayer; however, the relative changes, with regard to mechanical properties, between the undisturbed and disrupted regions of the bilayer would be similar.

Our results and simulations demonstrate that F_{min} and F_{max} of the tip/sample tapping force can be directly related to material properties of the surface. As a result, the mechanical properties of biological surfaces, such as lipid bilayers, can be mapped with nanoscale spatial resolution while simultaneously obtaining the surface topography in a tapping mode AFM experiment. Currently, this technique is limited to measuring relative shifts in properties within a single AFM image because of difficulties in controlling for variations in probe properties and imaging parameters. Despite these limitations, we have determined the morphological and mechanical changes associated with exposing lipid bilayers to amyloidogenic proteins. As membrane elasticity directly influences membrane stability, such mechanical changes can lead to membrane dysfunction and disease.[66] $A\beta_{1-40}$, htt exon1−51Q, synthetic polyQ peptide, and amylin all caused regions of morphological disruption of TBLE bilayers. While the extent and size of these regions varied,

disrupted regions of the bilayer had similar alterations in their mechanical properties. Specifically, these regions were more compressible and adhered more weakly to the AFM probe. The similar physical impact of these amyloid-forming proteins on bilayers suggests that this may represent an intrinsic amyloid–lipid interaction with potential implications for a common toxic mechanism.

■ ASSOCIATED CONTENT

Supporting Information

Image that demonstrates a "defect-free" 40 μm × 40 μm supported bilayer. This material is available free of charge via the Internet at http://pubs.acs.org.

■ AUTHOR INFORMATION

Corresponding Author

*Phone: (304) 293-0175. E-mail: justin.legleiter@mail.wvu.edu.

Author Contributions

K.A.B. and E.A.Y. contributed equally to this work.

Funding

This work was funded by the Brodie Discovery and Innovation Fund, the National Science Foundation (Grant 1054211), and the Alzheimer's Association (NIRG-11-203834).

Notes

The authors declare no competing financial interest.

■ ABBREVIATIONS

Aβ, β-amyloid peptide; AD, Alzheimer's disease; AFM, atomic force microscopy; APP, amyloid precursor protein; BSA, bovine serum albumin; DLVO, Derjaguin–Landau–Verway–Overbeek; DMSO, dimethyl sulfoxide; DMT, Derjaguin–Muller–Toporov; F_{max}, maximal tapping force; F_{min}, minimal tapping force; GST, glutathione *S*-transferase; HD, Huntington's disease; HFIP, hexafluoro-2-propanol; htt, huntingtin; PBS, phosphate-buffered saline; polyQ, polyglutamine; rms, root-mean-square; SPAM, scanning probe acceleration microscopy; TBLE, total brain lipid extract; TFA, trifluoroacetic acid.

■ REFERENCES

(1) Chiti, F., and Dobson, C. M. (2006) Protein Misfolding, Functional Amyloid, and Human Disease. *Annu. Rev. Biochem. 75*, 333–366.

(2) Selkoe, D. J. (2004) Cell biology of protein misfolding: The examples of Alzheimer's and Parkinson's diseases. *Nat. Cell Biol. 6*, 1054–1061.

(3) Vonsattel, J.-P., Myers, R. H., Stevens, T. J., Ferrante, R. J., Bird, E. D., and Richardson, E. P., Jr. (1985) Neuropathological classification of Huntington's disease. *J. Neuropathol. Exp. Neurol. 44*, 559–577.

(4) Hull, R., Westermark, G., Westermark, P., and Kahn, S. E. (2004) Islet amyloid: A critical entity in the pathogenesis of type 2 diabetes. *J. Clin. Endocrinol. Metab. 89*, 3629–3643.

(5) Jensen, M. O., and Mouritsen, O. G. (2004) Lipids do influence protein function: The hydrophobic matching hypothesis revisited. *Biochim. Biophys. Acta*, 205–226.

(6) Knight, J. D., and Miranker, A. D. (2004) Phospholipid catalysis of diabetic amyloid assembly. *J. Mol. Biol. 341*, 1175–1187.

(7) ChooSmith, L. P., GarzonRodriguez, W., Glabe, C. G., and Surewicz, W. K. (1997) Acceleration of amyloid fibril formation by specific binding of Aβ-(1–40) peptide to ganglioside-containing membrane vesicles. *J. Biol. Chem. 272*, 22987–22990.

(8) Yip, C. M., and McLaurin, J. (2001) Amyloid-β peptide assembly: A critical step in fibrillogenesis and membrane disruption. *Biophys. J. 80*, 1359–1371.

(9) McLaurin, J., and Chakrabartty, A. (1996) Membrane disruption by Alzheimer β-amyloid peptides mediated through specific finding to either phospholipids or gangliosides: Implications for neurotoxicity. *J. Biol. Chem. 271*, 26482–26489.

(10) McLaurin, J., and Chakrabartty, A. (1997) Characterization of the interactions of Alzheimer β-amyloid peptides with phospholipid membranes. *Eur. J. Biochem. 245*, 355–363.

(11) Yip, C. M., Elton, E. A., Darabie, A. A., Morrison, M. R., and McLaurin, J. (2001) Cholesterol, a modulator of membrane-associated Aβ-fibrillogenesis and neurotoxicity. *J. Mol. Biol. 311*, 723–734.

(12) Sparr, E., Engel, M. F. M., Sakharov, D. V., Sprong, M., Jacobs, J., de Kruijff, B., Hoppener, J. W. M., and Killian, J. A. (2004) Islet amyloid polypeptide-induced membrane leakage involves uptake of lipids by forming amyloid fibers. *FEBS Lett. 577*, 117–120.

(13) Thirumalai, D., Klimov, D. K., and Dima, R. I. (2003) Emerging ideas on the molecular basis of protein and peptide aggregation. *Curr. Opin. Struct. Biol. 13*, 146–159.

(14) Zhao, H. X., Tuominen, E. K. J., and Kinnunen, P. K. J. (2004) Formation of amyloid fibers triggered by phosphatidylserine-containing membranes. *Biochemistry 43*, 10302–10307.

(15) Kegel, K. B., Sapp, E., Alexander, J., Valencia, A., Reeves, P., Li, X., Masso, N., Sobin, L., Aronin, N., and DiFiglia, M. (2009) Polyglutamine expansion in huntingtin alters its interaction with phospholipids. *J. Neurochem. 110*, 1585–1597.

(16) Kegel, K. B., Sapp, E., Yoder, J., Cuiffo, B., Sobin, L., Kim, Y. J., Qin, Z. H., Hayden, M. R., Aronin, N., Scott, D. L., Isenberg, G., Goldmann, W. H., and DiFiglia, M. (2005) Huntingtin Associates with Acidic Phospholipids at the Plasma Membrane. *J. Biol. Chem. 280*, 36464–36473.

(17) Pifer, P. M., Yates, E. A., and Legleiter, J. (2011) Point mutations in Aβ result in the formation of distinct polymorphic aggregates in the presence of lipid bilayers. *PLoS One 6*, e16248.

(18) Domanov, Y. A., and Kinnunen, P. K. J. (2008) Islet Amyloid Polypeptide Forms Rigid Lipid-Protein Amyloid Fibrils on Supported Phospholipid Bilayers. *J. Mol. Biol. 376*, 42–54.

(19) Green, J. D., Kreplak, L., Goldsbury, C., Li Blatter, X., Stolz, M., Cooper, G. S., Seelig, A., Kistler, J., and Aebi, U. (2004) Atomic Force Microscopy Reveals Defects Within Mica Supported Lipid Bilayers Induced by the Amyloidogenic Human Amylin Peptide. *J. Mol. Biol. 342*, 877–887.

(20) Legleiter, J., Fryer, J. D., Holtzman, D. M., and Kowalewski, A. (2011) The modulating effect of mechanical changes in lipid bilayers caused by apoE-containing lipoproteins on Aβ induced membrane disruption. *ACS Chem. Neurosci. 2*, 588–599.

(21) Kinnunen, P. K. J. (2009) Amyloid Formation on Lipid Membrane Surfaces. *Open Biol. J. 2*, 163–175.

(22) Jang, H., Zheng, J., and Nussinov, R. (2007) Models of β-Amyloid Ion Channels in the Membrane Suggest That Channel Formation in the Bilayer Is a Dynamic Process. *Biophys. J. 93*, 1938–1949.

(23) Quist, A., Doudevski, L., Lin, H., Azimova, R., Ng, D., Frangione, B., Kagan, B., Ghiso, J., and Lal, R. (2005) Amyloid ion channels: A common structural link for protein-misfolding disease. *Proc. Natl. Acad. Sci. U.S.A. 102*, 10427–10432.

(24) Kegel, K., Kim, M., Sapp, E., McIntyre, C., Gastano, J., Aronin, N., and DiFiglia, M. (2000) Huntingtin expression stimulates endosomal-lysosomal activity, endosome tubulation, and autophagy. *J. Neurosci. 20*, 7268–7278.

(25) Orr, A. L., Li, S., Wang, C.-E., Li, H., Wang, J., Rong, J., Xu, X., Mastroberardino, P. G., Greenamyre, J. T., and Li, X.-J. (2008) N-Terminal Mutant Huntingtin Associates with Mitochondria and Impairs Mitochondrial Trafficking. *J. Neurosci. 28*, 2783–2792.

(26) Panov, A., Gutekunst, C.-A., Leavitt, B., Hayden, M., Burke, J., Strittmatter, W., and Greenamyre, J. (2002) Early mitochondrial calcium defects in Huntington's disease are a direct effect of polyglutamines. *Nat. Neurosci. 5*, 731–736.

(27) Qin, Z.-H., Wang, Y., Sapp, E., Cuiffo, B., Wanker, E., Hayden, M., Kegel, K., Aronin, N., and DiFiglia, M. (2004) Huntingtin bodies

sequester vesicle-associated proteins by a polyproline-dependent interaction. *J. Neurosci. 24*, 269−281.
(28) Suopanki, J., Götz, C., Lutsch, G., Schiller, J., Harjes, P., Herrmann, A., and Wanker, E. E. (2006) Interaction of huntingtin fragments with brain membranes: Clues to early dysfunction in Huntington's disease. *J. Neurochem. 96*, 870−884.
(29) Mirzabekov, T. A., Lin, M.-C., and Kagan, B. L. (1996) Pore Formation by the Cytotoxic Islet Amyloid Peptide Amylin. *J. Biol. Chem. 271*, 1988−1992.
(30) Last, N. B., Rhoades, E., and Miranker, A. D. (2011) Islet amyloid polypeptide demonstrates a persistent capacity to disrupt membrane integrity. *Proc. Natl. Acad. Sci. U.S.A. 108*, 9460−9465.
(31) Evangelisti, E., Cecchi, C., Cascella, R., Sgromo, C., Becatti, M., Dobson, C. M., Chiti, F., and Stefani, M. (2012) Membrane lipid composition and its physicochemical properties define cell vulnerability to aberrant protein oligomers. *J. Cell Sci. 125*, 2416−2427.
(32) Cecchi, C., Nichino, D., Zampagni, M., Bernacchioni, C., Evangelisti, E., Pensalfini, A., Liguri, G., Gliozzi, A., Stefani, M., and Relini, A. (2009) A protective role for lipid raft cholesterol against amyloid-induced membrane damage in human neuroblastoma cells. *Biochim. Biophys. Acta 1788*, 2204−2216.
(33) Stefani, M., and Liguri, G. (2009) Cholesterol in Alzheimer's Disease: Unresolved Questions. *Curr. Alzheimer Res. 6*, 15−29.
(34) Kim, D. H., and Frangos, J. A. (2008) Effects of amyloid β-peptides on the lysis tension of lipid bilayer vesicles containing oxysterols. *Biophys. J. 95*, 620−628.
(35) Bieschke, J., Herbst, M., Wiglenda, T., Friedrich, R. P., Boeddrich, A., Schiele, F., Kleckers, D., del Amo, J. M. L., Gruening, B. A., Wang, Q., Schmidt, M. R., Lurz, R., Anwyl, R., Schnoegl, S., Faendrich, M., Frank, R. F., Reif, B., Guenther, S., Walsh, D. M., and Wanker, E. E. (2012) Small-molecule conversion of toxic oligomers to nontoxic β-sheet-rich amyloid fibrils. *Nat. Chem. Biol. 8*, 93−101.
(36) Ehrnhoefer, D. E., Bieschke, J., Boeddrich, A., Herbst, M., Masino, L., Lurz, R., Engemann, S., Pastore, A., and Wanker, E. E. (2008) EGCG redirects amyloidogenic polypeptides into unstructured, off-pathway oligomers. *Nat. Struct. Mol. Biol. 15*, 558−566.
(37) Engel, M. F. M. (2009) Membrane Permeabilization by Islet Amyloid Polypeptide. *Chem. Phys. Lipids 160*, 1−10.
(38) Bokvist, M., Lindström, F., Watts, A., and Gröbner, G. (2004) Two Types of Alzheimer's β-Amyloid (1−40) Peptide Membrane Interactions: Aggregation Preventing Transmembrane Anchoring Versus Accelerated Surface Fibril Formation. *J. Mol. Biol. 335*, 1039−1049.
(39) Atwal, R. S., Xia, J., Pinchev, D., Taylor, J., Epand, R. M., and Truant, R. (2007) Huntingtin has a membrane association signal that can modulate huntingtin aggregation, nuclear entry and toxicity. *Hum. Mol. Genet. 16*, 2600−2615.
(40) Williamson, J. A., Loria, J. P., and Miranker, A. D. (2009) Helix Stabilization Precedes Aqueous and Bilayer-Catalyzed Fiber Formation in Islet Amyloid Polypeptide. *J. Mol. Biol. 393*, 383−396.
(41) Legleiter, J., Park, M., Cusick, B., and Kowalewski, T. (2006) Scanning probe acceleration microscopy (SPAM) in fluids: Mapping mechanical properties of surfaces at the nanoscale. *Proc. Natl. Acad. Sci. U.S.A. 103*, 4813−4818.
(42) Stine, W. B., Dahlgren, K. N., Krafft, G. A., and LaDu, M. J. (2003) In Vitro Characterization of Conditions for Amyloid-β Peptide Oligomerization and Fibrillogenesis. *J. Biol. Chem. 278*, 11612−11622.
(43) Cho, W. J., Jena, B. P., and Jeremic, A. M. (2008) Nano-scale imaging and dynamics of amylin-membrane interactions and its implication in type II diabetes mellitus. *Methods Cell Biol. 90*, 267−286.
(44) Reddy, A. S., Wang, L., Singh, S., Ling, Y. L., Buchanan, L., Zanni, M. T., Skinner, J. L., and de Pablo, J. J. (2010) Stable and metastable states of human amylin in solution. *Biophys. J. 99*, 2208−2216.
(45) Burke, K. A., Godbey, J., and Legleiter, J. (2011) Assessing mutant huntingtin fragment and polyglutamine aggregation by atomic force microscopy. *Methods 53*, 275−284.
(46) Muchowski, P. J., Schaffar, G., Sittler, A., Wanker, E. E., Hayer-Hartl, M. K., and Hartl, F. U. (2000) Hsp70 and Hsp40 chaperones can inhibit self-assembly of polyglutamine proteins into amyloid-like fibrils. *Proc. Natl. Acad. Sci. U.S.A. 97*, 7841−7846.
(47) Chen, S., and Wetzel, R. (2001) Solubilization and disaggregation of polyglutamine peptides. *Protein Sci. 10*, 887−891.
(48) Hutter, J. L., and Bechhoefer, J. (1993) Calibration of atomic force microscope tips. *Rev. Sci. Instrum. 64*, 1868−1873.
(49) Kuhle, A., Sorensen, A. H., and Bohr, J. (1997) Role of attractive forces in tapping tip force microscopy. *J. Appl. Phys. 81*, 6562−6569.
(50) Salapaka, M. V., Chen, D. J., and Cleveland, J. P. (2000) Linearity of amplitude and phase in tapping-mode atomic force microscopy. *Phys. Rev. B 61*, 1106.
(51) Israelachvili, J. N. (1991) *Intermolecular and surface forces*, Academic Press, San Diego.
(52) Xu, X., Carrasco, C., de Pablo, P. J., Gomez-Herrero, J., and Raman, A. (2008) Unmasking imaging forces on soft biological samples in liquids when using dynamic atomic force microscopy: A case study on viral capsids. *Biophys. J. 95*, 2520−2528.
(53) Israelachvili, J., and Wennerstrom, H. (1996) Role of hydration and water structure in biological and colloidal interactions. *Nature 379*, 219−225.
(54) Derjaguin, B. V., Muller, V. M., and Toporov, Y. P. (1975) Effect of contact deformations on the adhesion of particles. *J. Colloid Interface Sci. 53*, 314−326.
(55) Kumar, B., Pifer, P. M., Giovengo, A., and Legleiter, J. (2010) The effect of set point ratio and surface Young's modulus on maximum tapping forces in fluid tapping mode atomic force microscopy. *J. Appl. Phys. 107*, 044508.
(56) Legleiter, J., and Kowalewski, T. (2005) Insights into fluid tapping-mode atomic force microscopy provided by numerical simulations. *Appl. Phys. Lett. 87*, 163120−163123.
(57) Jass, J., Tjarnhage, T., and Puu, G. (2000) From liposomes to supported, planar bilayer structures on hydrophilic and hydrophobic surfaces: An atomic force microscopy study. *Biophys. J. 79*, 3153−3163.
(58) Hepler, R. W., Grimm, K. M., Nahas, D. D., Breese, R., Dodson, E. C., Acton, P., Keller, P. M., Yeager, M., Wang, H., Shughrue, P., Kinney, G., and Joyce, J. G. (2006) Solution State Characterization of Amyloid β-Derived Diffusible Ligands. *Biochemistry 45*, 15157−15167.
(59) Cheng, I. H., Scearce-Levie, K., Legleiter, J., Palop, J. J., Gerstein, H., Bien-Ly, N., Puolivali, J., Lesne, S., Ashe, K. H., Muchowski, P. J., and Mucke, L. (2007) Accelerating amyloid-β fibrillization reduces oligomer levels and functional deficits in Alzheimer disease mouse models. *J. Biol. Chem. 282*, 23818−23828.
(60) Legleiter, J., Mitchell, E., Lotz, G. P., Sapp, E., Ng, C., DiFiglia, M., Thompson, L. M., and Muchowski, P. J. (2010) Mutant huntingtin fragments form oligomers in a polyglutamine length-dependent manner in vitro and in vivo. *J. Biol. Chem. 285*, 14777−14790.
(61) Sathasivam, K., Lane, A., Legleiter, J., Warley, A., Woodman, B., Finkbeiner, S., Paganetti, P., Muchowski, P. J., Wilson, S., and Bates, G. P. (2010) Identical oligomeric and fibrillar structures captured from the brains of R6/2 and knock-in mouse models of Huntington's disease. *Hum. Mol. Genet. 19*, 65−78.
(62) Weise, K., Radovan, D., Gohlke, A., Opitz, N., and Winter, R. (2010) Interaction of hIAPP with Model Raft Membranes and Pancreatic β-Cells: Cytotoxicity of hIAPP Oligomers. *ChemBioChem 11*, 1280−1290.
(63) Evers, F., Jeworrek, C., Tiemeyer, S., Weise, K., Sellin, D., Paulus, M., Struth, B., Tolan, M., and Winter, R. (2009) Elucidating the Mechanism of Lipid Membrane-Induced IAPP Fibrillogenesis and Its Inhibition by the Red Wine Compound Resveratrol: A Synchrotron X-ray Reflectivity Study. *J. Am. Chem. Soc. 131*, 9516−9521.
(64) Duan, M. J., Fan, J., and Huo, S. H. (2012) Conformations of Islet Amyloid Polypeptide Monomers in a Membrane Environment: Implications for Fibril Formation. *PLoS One 7*, No. e47150.
(65) Hong, H., and Tamm, L. K. (2004) Elastic coupling of integral membrane protein stability to lipid bilayer forces. *Proc. Natl. Acad. Sci. U.S.A. 101*, 4065−4070.

(66) Vogel, V., and Sheetz, M. (2006) Local force and geometry sensing regulate cell functions. *Nat. Rev. Mol. Cell Biol. 7*, 265−275.
(67) Janmey, P. A., and Weitz, D. A. (2004) Dealing with mechanics: Mechanisms of force transduction in cells. *Trends Biochem. Sci. 29*, 364−370.
(68) Ambroggio, E. E., Kim, D. H., Separovic, F., Barrow, C. J., Barnham, K. J., Bagatolli, L. A., and Fidelio, G. D. (2005) Surface Behavior and Lipid Interaction of Alzheimer *β*-Amyloid Peptide 1−42: A Membrane-Disrupting Peptide. *Biophys. J. 88*, 2706−2713.
(69) Demuro, A., Mina, E., Kayed, R., Milton, S. C., Parker, I., and Glabe, C. G. (2005) Calcium Dysregulation and Membrane Disruption as a Ubiquitous Neurotoxic Mechanism of Soluble Amyloid Oligomers. *J. Biol. Chem. 280*, 17294−17300.
(70) Choo, Y. S., Johnson, G. V. W., MacDonald, M., Detloff, P. J., and Lesort, M. (2004) Mutant huntingtin directly increases susceptibility of mitochondria to the calcium-induced permeability transition and cytochrome c release. *Hum. Mol. Genet. 13*, 1407−1420.
(71) Lorenzo, A., Razzaboni, B., Weir, G. C., and Yankner, B. A. (1994) Pancreatic islet cell toxicity of amylin associated with type-2 diabetes mellitus. *Nature 368*, 756−760.
(72) Lim, Y.-A., Rhein, V., Baysang, G., Meier, F., Poljak, A., Raftery, M. J., Guilhaus, M., Ittner, L. M., Eckert, A., and Götz, J. (2010) A*β* and human amylin share a common toxicity pathway via mitochondrial dysfunction. *Proteomics 10*, 1621−1633.
(73) Dong, M., Husale, S., and Sahin, O. (2009) Determination of protein structural flexibility by microsecond force spectroscopy. *Nat. Nanotechnol. 4*, 514−517.
(74) Sahin, O. (2007) Harnessing bifurcations in tapping-mode atomic force microscopy to calibrate time-varying tip-sample force measurements. *Rev. Sci. Instrum. 78*, 103707.
(75) Sahin, O. (2008) Time-varying tip-sample force measurements and steady-state dynamics in tapping-mode atomic force microscopy. *Phys. Rev. B 77*, 115405.
(76) Sahin, O., and Erina, N. (2008) High-resolution and large dynamic range nanomechanical mapping in tapping-mode atomic force microscopy. *Nanotechnology 19*, 445717.
(77) Xu, X., Melcher, J., Basak, S., Reifenberger, R., and Raman, A. (2009) Compositional Contrast of Biological Materials in Liquids Using the Momentary Excitation of Higher Eigenmodes in Dynamic Atomic Force Microscopy. *Phys. Rev. B 102*, 060801−060804.
(78) Stark, M., Stark, R. W., Heckl, W. M., and Guckenberger, R. (2002) Inverting dynamic force microscopy: From signals to time-resolved interaction forces. *Proc. Natl. Acad. Sci. U.S.A. 99*, 8473−8478.
(79) Stark, R. W., and Heckl, W. M. (2003) Higher harmonics imaging in tapping-mode atomic-force microscopy. *Rev. Sci. Instrum. 74*, 5111−5114.
(80) Garcia, R., and Herruzo, E. T. (2012) The emergence of multifrequency force microscopy. *Nat. Nanotechnol. 7*, 217−226.
(81) Cantor, R. S. (1997) The lateral pressure profile in membranes: A physical mechanism of general anesthesia. *Biochemistry 36*, 2339−2344.
(82) Cantor, R. S. (1997) Lateral Pressures in Cell Membranes: A Mechanism for Modulation of Protein Function. *J. Phys. Chem. B 101*, 1723−1725.
(83) Johnson, S. J., Bayerl, T. M., McDermott, D. C., Adam, G. W., Rennie, A. R., Thomas, R. K., and Sackmann, E. (1991) Structure of an Adsorbed Dimyristoylphosphatidylcholine Bilayer Measured with Specular Reflection of Neutrons. *Biophys. J. 59*, 289−294.
(84) Koenig, B. W., Kruger, S., Orts, W. J., Majkrzak, C. F., Berk, N. F., Silverton, J. V., and Gawrisch, K. (1996) Neutron reflectivity and atomic force microscopy studies of a lipid bilayer in water adsorbed to the surface of a silicon single crystal. *Langmuir 12*, 1343−1350.
(85) Mager, M., Almquist, B., and Melosh, N. (2008) Formation and Characterization of Fluid Lipid Bilayers on Alumina. *Langmuir 24*, 12734−12737.
(86) Kuhner, M., Tampe, R., and Sackmann, E. (1994) Lipid mono- and bilayer supported on polymer films: Composite polymer-lipid films on solid substrates. *Biophys. J. 67*, 217−226.
(87) Shamitko-Klingensmith, N., Molchanoff, K. M., Burke, K. A., Magnone, G. J., and Legleiter, J. (2012) Mapping the Mechanical Properties of Cholesterol-Containing Supported Lipid Bilayers with Nanoscale Spatial Resolution. *Langmuir 28*, 13411−13422.

Supporting Information for:

Amyloid-forming proteins alter the local mechanical properties of lipid membranes

Funding Source Statement: This work was funded by the Brodie Discovery and Innovation fund, the National Science Foundation (NSF#1054211), and the Alzheimer's Association (NIRG-11-203834).

Kathleen A. Burke[1#], Elizabeth A. Yates[1#], and Justin Legleiter[1,2,3,*]

[1]The C. Eugene Bennett Department of Chemistry; [2]WVnano Initiative; [3]the Center for Neurosciences, West Virginia University, Morgantown, WV 26505, USA.

[#]These authors contributed equally to this project.

[*]Corresponding author:

Justin Legleiter

Phone: 304-293-0175

Email: justin.legleiter@mail.wvu.edu

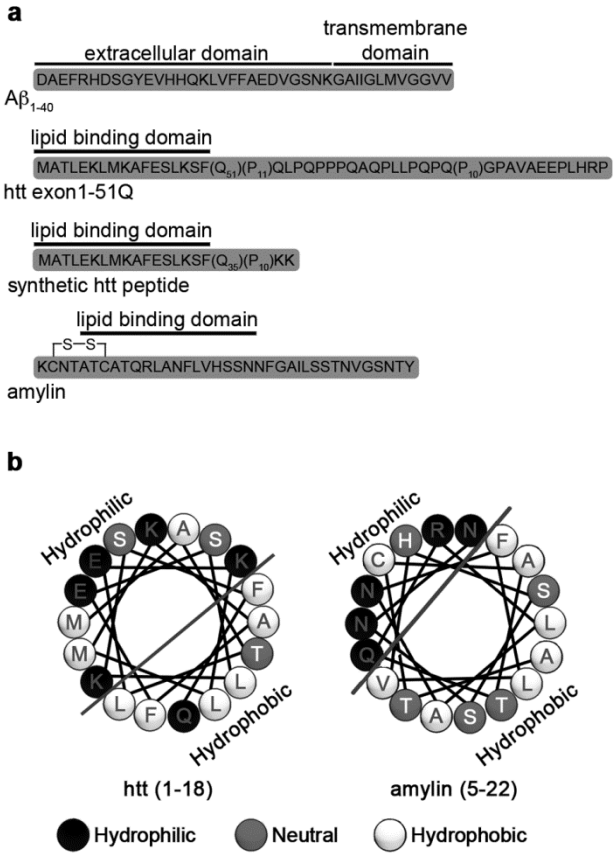

Figure S1: Schematic representations of the amyloid-forming proteins. a) The primary sequences of $A\beta_{1\text{-}40}$, htt exon1-51Q, a synthetic polyQ peptide, and amylin are shown with important domains within the protein indicated. b) The lipid binding domains of htt and amylin form amphipathic α-helixes.

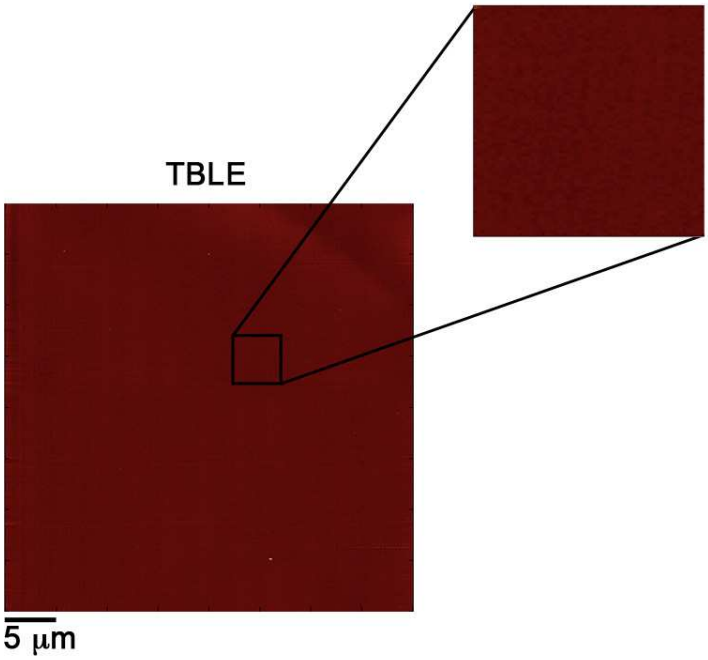

Figure S2. AFM image of a representative, relatively defect-free TBLE bilayer supported on mica. The image represents a 40 x 40 μm area, and the inset zooms into a 5 x 5 μm area. Holes and defects of the size detectable by AFM are relativley few, if any.

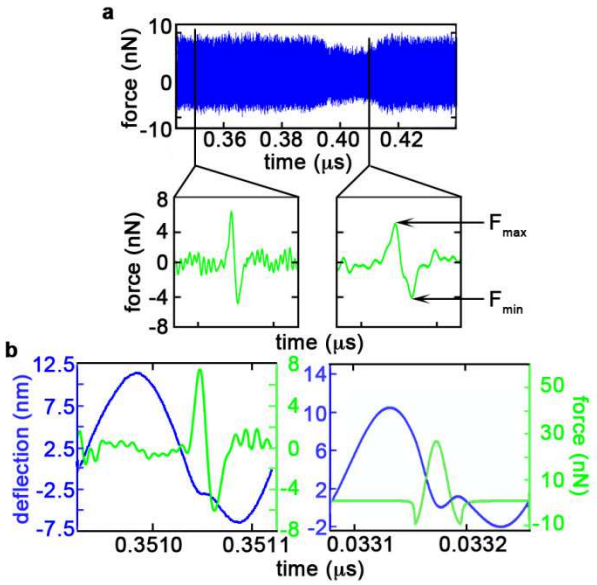

Figure S3. Comparison between experimental and simulated cantilever deflection trajectories and tip/sample forces. a) The time-resolved tip/sample force trajectory associated with imaging a lipid bilayer exposed to amyloid-forming proteins. Example force interaction for one oscillation cycle are shown, with F_{max} and F_{min} indicated. b) Experimental (left) and simulated (right) cantilever deflection and tapping force trajectories are shown.

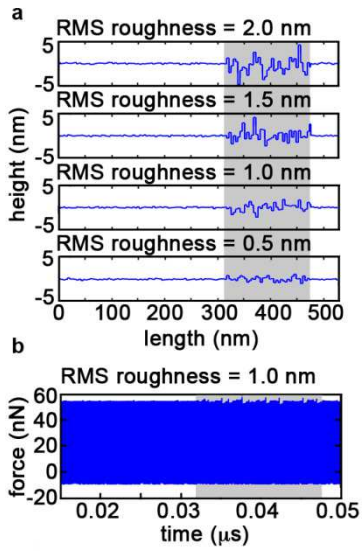

Figure S4: Numerical simulations exploring the relationship between tapping forces and surface roughenss. a) Simulated height profiles are shown with regions of increased root-mean-square (RMS) roughness (indicated by gray shading) ranging from 0.5 to2.0 nm. b) A representative, simulated force trajectory associated with imaging a surface inwhich the RMS roughness increased in the variable region of the model surface (from 0.1 to 2.0nm).

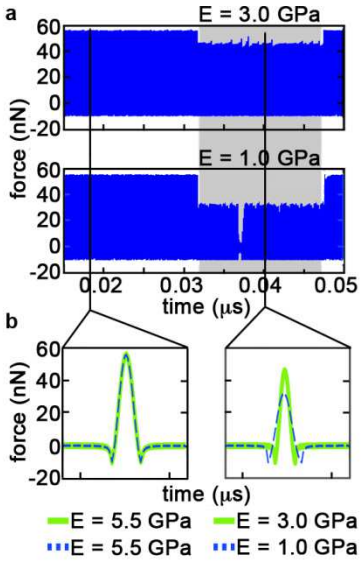

Figure S5: Numerical simulations exploring the relationship between tapping forces and surface Young's modulus. a) Simulated force trajectories associated with imaging a surface with the Young's modulus changing from 5.5 GPa to 3.0 GPa or 1.0 GPa (shaded in gray) respectively. b) Tip/sample force for one oscillation cycle for simulations with different values of Young's modulus as indicated.

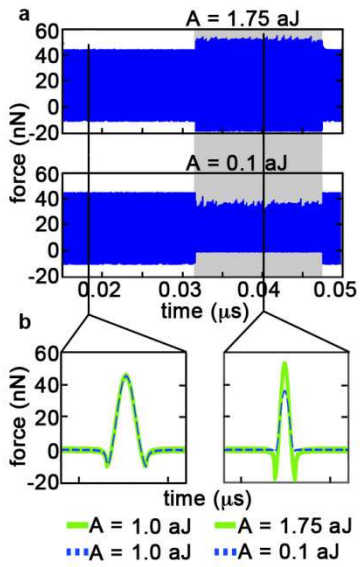

Figure S6: Numerical simulations exploring the relationship between tapping forces and surface Young's modulus. a) Simulated force trajectories associated with imaging a surface with the Hamaker constant changing from 1.0 a J to 1.75 a J or 0.1 a J (shaded in gray) respectively. b) Tip/sample force for one oscillation cycle for simulations with different values of the Hamaker constant as indicated.